The deformation of an elastic cell in a circulatory fluid motion

A. A. Yorkston, M. G. Blyth, & E. I. Părău

Abstract

The deformation of a two-dimensional inextensible elastic cell in an inviscid uniform stream with circulation is investigated. An asymptotic expansion based on a conformal mapping is used to obtain equilibria for low far-field flow speeds, and fully nonlinear solutions are obtained numerically. Expanding upon the results of Blyth & Părău [1] and Yorkston *et al.* [2] for an elastic cell in a uniform stream with zero circulation, it is shown that the nature of the cell deformation in response to circulation depends on whether the transmural pressure exceeds a series of critical values. Below the first of these critical values, the deformed cell is elongated vertically against the stream, and the circulation acts to reduce the deformation of the cell from the circular rest-state, while above this critical pressure the deformed cell elongates horizontally parallel to the flow, with stronger circulation resulting in more severe cell deformation until self-intersection. The solution branches which emerge at the second critical transmural pressure are found to form a closed loop in parameter space, which shrinks in size as the circulation is increased to a critical value at which the solution branch vanishes. We also present a set solution branches distinct from those found by Yorkston *et al.* [2], which become dominant for large values of circulation.

1. Introduction

The deformation of an elastic body in response to hydrodynamic forces is a problem with applications in many fields. In biomechanics, elastic cells have been used to model the deformation of blood cells [3, 4] and capsules used for drug delivery [5], while in the aerospace industry there is increasing interest in the use of inflatable aerofoils which deform elastically in response to the airflow [6, 7, 8].

The deformation of an elastic cell that is positioned in an inviscid uniform stream in the absence of circulation has been well studied. The deformation of an elastic cell subject to constant transmural pressure was analysed by Lévy [9], Carrier [10] and Tadjbakhsh & Odeh [11], and subsequently expanded on by Flaherty *et al.* [12] to account for an interval of self-contact. Blyth & Părău [1] used a conformal mapping approach to show that a cell in a uniform stream will deform into an ellipse-like shape, with its orientation determined by whether the transmural pressure exceeds the first of the critical values identified by Halphen [13] at which elastic cells buckle in a static fluid. Yorkston *et al.* [2] subsequently used an asymptotic expansion based on a conformal mapping to obtain distinct solutions which bifurcate at each of the critical pressures of Halphen [13], and presented a detailed analysis of the solution space.

The work of Blyth & Părău [1] and Yorkston *et al.* [2] builds upon results obtained for the closely related problem of the deformation of a bubble in an inviscid flow (the current problem is reduced to the bubble problem under the appropriate limit). Vanden-Broeck & Keller [14] obtained numerical solutions for a uniform stream by formulating the problem as an integrodifferential equation, while Shankar [15] used a conformal mapping method to obtain asymptotic solutions for low flow speeds, and Nie & Tanveer [16] performed a linear stability analysis for the deformed bubble shapes. Exact solutions

for a circulatory flow were obtained by Crowdy [17], and expanded upon by Wegmann & Crowdy [18].

Here we conduct a study of the deformation of an elastic cell in an inviscid uniform stream with circulation. Guided by the results of Yorkston *et al.* [2], we use an asymptotic expansion based on the conformal mapping technique of Shankar [15] to obtain analytic expressions for solutions at low flow speeds, identifying a set of novel solution branches which only exist for non-zero circulation. We use numerical methods to extend the solution branches to arbitrary flow speeds, and analyse the effects of circulation on the solutions.

2. Formulation

We consider the deformation of a closed, two dimensional elastic cell placed in an inviscid, incompressible, irrotational fluid flow. The cell wall is assumed to be inextensible with constant thickness h and uniform density ρ_c, and in the absence of an external pressure the cell is assumed to take the shape of a circle. The fluid in the exterior of the cell is taken to be a horizontal uniform stream of speed U in the far-field with circulation Γ around the cell. The interior of the cell is assumed to be a static fluid of density ρ equal to that of the exterior fluid.

For equilibria to occur the lift force acting upon the cell must be balanced by the weight of the cell material. The density of the cell material can thus be obtained from the Kutta-Joukowski theorem as

$$\rho_c = -\frac{\rho U \Gamma}{2\pi g h \ell}. \tag{2.1}$$

For physical solutions we thus require $U\Gamma \leq 0$, which ensures that the lift force acts in the upwards direction.

A balance of forces acting upon the cell wall is given by

$$\frac{\mathrm{d}}{\mathrm{d}s}\Big(T(s)\hat{\boldsymbol{\tau}} + N(s)\hat{\boldsymbol{n}}\Big) - \rho_c h g \boldsymbol{j} + \Delta p(s)\hat{\boldsymbol{n}} = 0, \tag{2.2}$$

where $\hat{\boldsymbol{\tau}}$ and $\hat{\boldsymbol{n}}$ are unit vectors in the anticlockwise tangential and outward normal directions respectively, s is the arc-length of the cell wall in the anticlockwise direction, g is the acceleration due to gravity, $\Delta p(s)$ is the difference between the interior and exterior fluid pressures acting on the cell wall, and $N(s)$ and $T(s)$ are the normal and tangential components respectively of the internal tension.

We assume the bending moment at any point is proportional to the difference between the curvature at that point and its resting curvature. Such an assumption is justified by [19] for a locally inextensible cell. This gives the constitutive equation for the bending moment

$$M = -E_B(\kappa - \kappa_R), \tag{2.3}$$

where $\kappa(s)$ is the signed curvature of the cell, κ_R is the resting curvature, which is assumed to be constant, and E_B is the bending modulus. According to thin-shell theory, the bending modulus is given by $E_B = \frac{Eh^3}{12(1-\nu^2)}$, where E is the Young's modulus of the cell-wall, ν is the Poisson's ratio of the cell-wall, and h is the thickness of the cell-wall. A balancing of moments about an infinitesimal section of the cell wall thus gives $N = M_s = -E_B \kappa_s$. Splitting (2.2) into tangential and normal components, we obtain

$$T_s + E_B \kappa \kappa_s - \rho_c h g y_s = 0, \quad -E_B \kappa_{ss} + \kappa T + \rho_c h g x_s + \Delta p(s) = 0, \tag{2.4}$$

2

where $x(s)$ and $y(s)$ are the horizontal and vertical components respectively of the arc-length parameterisation of the cell boundary. Integrating (2.4), we obtain

$$\Delta p(s) = E_B\left(\kappa_{ss} + \frac{1}{2}\kappa^3 - \frac{\sigma\kappa}{\ell^2}\right) - \rho_c hg(x_s + \kappa y), \tag{2.5}$$

where ℓ is a length scale taken to be the radius of the undeformed cell, and σ is some undetermined constant.

The fluid pressure difference across the cell boundary is given by Bernoulli's equation as

$$\Delta p(s) = p_0 - p_\infty + \frac{1}{2}\rho\left(q(s)^2 - U^2\right), \tag{2.6}$$

where p_0 and p_∞ are the fluid pressures in the interior of the cell and in the far-field respectively, and $q = |\partial w/\partial z|$ is the flow speed evaluated at the cell boundary. Substituting into 2.5 and nondimensionalising using the length scale ℓ, the radius of the undeformed cell, and the velocity scale $\sqrt{E_B/(\ell^3\rho)}$, we obtain

$$\frac{1}{2}(q^2 - \alpha^2) - (\kappa_{ss} + \frac{1}{2}\kappa^3 - \sigma\kappa) + \frac{\alpha\beta}{2\pi}(x_s + \kappa y) - P = 0, \tag{2.7}$$

where all variables are now dimensionless. The dimensionless parameters are defined as

$$\alpha = U\sqrt{\frac{\ell^3\rho}{E_B}}, \quad \beta = -\Gamma\sqrt{\frac{\ell\rho}{E_B}}, \quad P = \frac{(p_\infty - p_0)\ell^3}{E_B}$$

which relate to the far-field flow speed, the circulation around the cell, and the pressure difference between far-field and the interior of the cell respectively. Note that the sign of β has been chosen such that a positive value of β corresponds to an upwards lift force.

The dimensionless bending energy of the cell is given by

$$\mathscr{W} = \int_0^{2\pi} \tfrac{1}{2}(\kappa + 1)^2 \mathrm{d}s, \tag{2.8}$$

where the resting cell with curvature $\kappa = -1$ has zero bending energy.

The flow field in the exterior of the cell is obtained using the conformal mapping of Shankar [15], which maps to the exterior of the cell in the complex z-plane from the exterior of the unit circle in some ζ-plane. This mapping can be written as

$$z(\zeta) = a_{-1}\left(\zeta + \sum_{n=1}^\infty a_n \zeta^{-n}\right), \tag{2.9}$$

where the coefficients a_n are generally complex. Parametrising the unit circle in the ζ-plane as $\zeta = \mathrm{e}^{\mathrm{i}\phi}$, where $0 \le \phi < 2\pi$, the cell wall is then given in complex form as

$$\eta(\phi) = a_{-1}\left(\mathrm{e}^{\mathrm{i}\phi} + \sum_{n=1}^\infty a_n e^{-\mathrm{i}n\phi}\right). \tag{2.10}$$

The coefficient a_{-1} is taken to be

$$a_{-1} = \frac{2\pi}{\int_0^{2\pi} |\eta_\phi|\mathrm{d}\phi}, \tag{2.11}$$

which ensures that the perimeter of the cell is equal to 2π. In the pre-mapped ζ-plane the complex potential is given by

$$w(\zeta) = \alpha a_{-1}\left(\zeta + \frac{1}{\zeta}\right) - \frac{\beta}{2\pi\mathrm{i}}\log\zeta \tag{2.12}$$
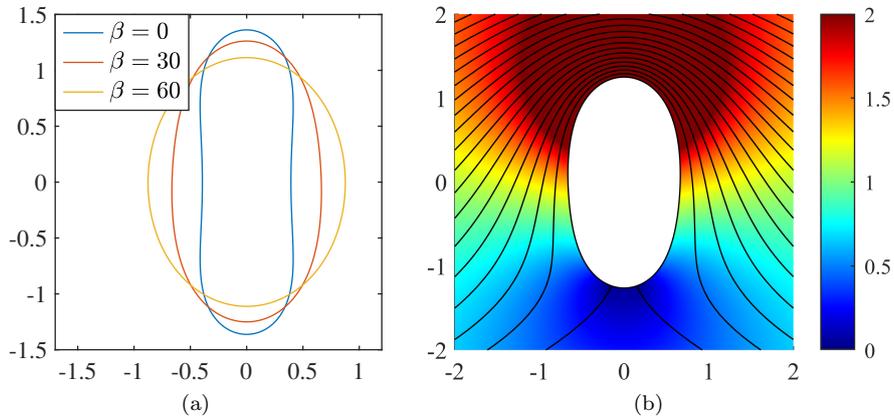
3

Figure 1: Numerically computed cell shapes for $\alpha = 2.5$, $P = 0$. (a) shows the cell shape for various values of the circulation β. (b) shows a contour plot of the flow past the cell for $\beta = 30$, with the colour scale corresponding to the flow speed divided by the far-field flow speed α. The black lines are the streamlines of the flow.

which gives the flow speed at the cell wall as

$$q(\phi) = \left\| \frac{\mathrm{d}w}{\mathrm{d}z} \right\|_{\zeta=e^{\mathrm{i}\phi}} = \left| \frac{2\alpha a_{-1}\sin\phi + \beta/2\pi}{\eta_\phi} \right|. \tag{2.13}$$

We note that (2.12) has stagnation points located at

$$\zeta = \pm\sqrt{1 - \left(\frac{\beta}{4\pi\alpha a_{-1}}\right)^2} - \frac{\beta\mathrm{i}}{4\pi\alpha a_{-1}}. \tag{2.14}$$

Thus for $0 < \beta < 4\pi\alpha a_{-1}$ there are two stagnation points located on the cell boundary, while for $\beta > 4\pi\alpha a_{-1}$ there exists a single stagnation point in the flow, away from the cell boundary.

Finally, substituting (2.13) into (2.7), we obtain the single governing equation

$$\frac{1}{2}\left(\left|\frac{2\alpha a_{-1}\sin\phi + \beta/2\pi}{\eta_\phi}\right|^2 - \alpha^2\right) - P - \left(\kappa_{ss} + \frac{1}{2}\kappa^3 - \sigma\kappa\right)$$
$$+ \frac{\alpha\beta}{2\pi}(x_s + \kappa y) = 0, \tag{2.15}$$

to be solved for the values of the mapping coefficients a_n.

3. Numerical Method

The numerical method used to compute nonlinear equilibria is based on that presented by Tanveer [20]. We truncate the Fourier series (2.10) at N terms, taking $a_n = 0$ for $n > N$. We then split up the coefficients into the $2N$ real variables $\Re(a_n)$ and $\Im(a_n)$ for $1 \leq n \leq N$, with a_{-1} given in terms of a_n by (2.11). The parameters α and P are freely chosen, while σ is to be found as part of the solution. We obtain explicit expressions for κ and κ_{ss} for the truncated mapping in terms of the mapping coefficients a_n and evaluate (2.15) at $2N + 1$ equally spaced collocation points $\phi_i = 2\pi(i-1)/(2N+1)$

4

for $i = 1, \ldots, 2N + 1$, giving $2N + 1$ equations to solve for the $2N + 1$ variables. We obtain the Jacobian of the truncated system analytically, and Newton's method can be used to obtain a numerical solution. For the results shown in this section we generally take $N = 200$, although values as high as $N = 2000$ are required for certain solutions. To confirm the accuracy of the numerical results we note that, for any given mapping function, the absolute value of the left-hand side of (2.15) can be obtained analytically along the entire cell, not just at the $2N+1$ collocation points used in Newton's method. We can therefore verify the validity of our results by sampling (2.15) at a much larger number of points, say $1000N$, and confirm that the maximum value remains below some tolerance level; all results in this chapter have a maximum absolute error less than 10^{-10}. We use the small α asymptotic results presented below as an initial guess for Newton's method. The full nonlinear solution space can then be explored by continuation in the parameters α and P.

4. Results

It is well known that in the absence of a far-field flow, corresponding to $\alpha = 0$, there exists a trivial circular cell solution for all values of β. [1] showed that, as well as these trivial solutions, there exist a set of buckled mode-k symmetric cells which bifurcate from the circular solution as the pressure P passes through a set of critical pressures

$$P_k(\beta) = k^2 - 1 + \frac{k-1}{k+1}\frac{\beta^2}{8\pi^2}. \tag{4.1}$$

We seek solutions for $\alpha > 0$ which bifurcate from the trivial circular solution at $\alpha = 0$ by expanding the unknowns a_n and σ as asymptotic series in α of the form

$$a_n = a_{n,1}\alpha + a_{n,2}\alpha^2 + \mathcal{O}(\alpha^3) \quad n \geq 1, \tag{4.2}$$

$$\sigma = \tfrac{1}{2} - P + \tfrac{1}{8\pi^2}\beta^2 + \sigma_1\alpha + \sigma_2\alpha^2 + \mathcal{O}(\alpha^3). \tag{4.3}$$

Substituting these expansions into (2.15) and evaluating at $\mathcal{O}(\alpha)$, we obtain

$$-\sigma_1 + \sum_{n=2}^{\infty}(n^2 - 1)(P - P_n(\beta))\Re(a_{n-1,1}e^{-in\phi}) = 0, \tag{4.4}$$

where $P_n(\beta)$ is the nth critical pressure given by (4.1). We thus require $\sigma_1 = 0$, and for each $n \geq 2$ we require either $a_{n-1,1} = 0$ or $P = P_n(\beta)$. We split the problem into two distinct cases; we start by looking for a solution which is valid for general values of P, where $P \neq P_k(\beta)$ for all $k \geq 2$. We then look for solutions which are valid at each of the critical pressures $P = P_k(\beta)$ for $k \geq 2$.

First seeking a solution valid for general values of P, we assume $P \neq P_k$ for all $k \geq 2$. Equation (4.4) thus gives $\sigma_1 = 0$ and $a_{n,1} = 0$ for all $n \geq 1$. Next satisfying (2.15) at $\mathcal{O}(\alpha^2)$, we obtain

$$\tfrac{1}{2} - \sigma_2 - \cos(2\phi) + \sum_{n=2}^{\infty}(n^2 - 1)(P - P_n(\beta))\Re(a_{n-1,2}e^{-in\phi}) = 0. \tag{4.5}$$

Noting that

$$\Re(a_{n-1,2}e^{-in\phi}) = \Re(a_{n-1,2})\cos(n\phi) + \Im(a_{n-1,2})\sin(n\phi),$$

we compare coefficients of $\cos(n\phi)$ and $\sin(n\phi)$ in (4.5) to obtain
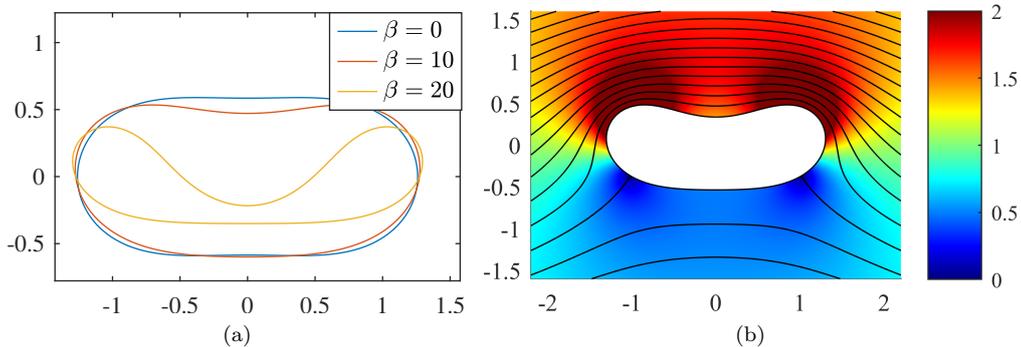
$$a_{1,2} = \frac{1}{3(P - P_2)}$$

5

Figure 2: Numerically computed cell shapes for $\alpha = 2.5$, $P = 6$. (a) shows the cell shape for various values of the circulation β. (b) shows a contour plot of the flow past the cell for $\beta = 15$, with the colour scale corresponding to the flow speed divided by the far-field flow speed α. The black lines are the streamlines of the flow.

and $a_{n,2} = 0$ for $n \geq 2$, with $\sigma_2 = \frac{1}{2}$. We then proceed in the same way to higher powers of α using the symbolic computing environment Maple to obtain

$$\eta(\phi) = e^{i\phi} + \frac{1}{3(P - P_2)}\alpha^2 e^{-i\phi} + \mathcal{O}(\alpha^4), \tag{4.6}$$

an ellipse which is elongated vertically for $P < P_2$ and horizontally for $P > P_2$. Note that setting $\beta = 0$ reduces this solution to that obtained by [2]. However, unlike the $\beta = 0$ solution, the coefficients a_2 and a_4 are imaginary for $\beta \neq 0$, causing the cell to lose its top-bottom symmetry, although the cell remains left-right symmetric. This solution becomes invalid when the pressure P is equal to any of the critical pressures $P_k(\beta)$. This contrasts with the $\beta = 0$ solutions, which are only invalid for $P = P_{2k}$ while remaining valid for $P = P_{2k+1}$. This suggests that the general solution branch valid for $\beta = 0$ and $P = P_{2k+1}$ detaches from $\alpha = 0$ as circulation is introduced; the exact nature of this behaviour will be discussed further on.

Figures 1 and 2 show numerically computed cell shapes for $P = 0$ and $P = 6$ respectively for various values of β, along with a plot of the flow field for $\beta = 30$. For $P = 0$ the cell is elongated vertically, as predicted by (4.6). As β is increased the cell deformation decreases and the cell becomes more circular. This agrees with (4.6); as β is increased the critical pressure $P_2(\beta)$ increases, and so the magnitude of the factor $\frac{1}{3(P - P_2)}$ decreases, resulting in a more circular cell shape. For $P = 6$ the cell is oriented horizontally, which also agrees with (4.6). As β is increased, the magnitude of the factor $\frac{1}{3(P - P_2)}$ in (4.6) increases, resulting in a more elongated cell shape. This deformation increases with β until the cell eventually self-intersects, at which point the solution becomes physically invalid.

We then seek asymptotic solutions which are valid at the critical pressures $P = P_k(\beta)$, focussing in particular on the first two critical pressure $P_2(\beta)$ and $P_3(\beta)$. We start by considering the case where $P = P_2(\beta) = 3 + \beta^2/(24\pi)$. As shown by [1] for the case of $\beta = 0$, we find that (2.15) cannot be satisfied by an expansion in integer powers of α. We instead take an expansion in powers of $\alpha^{1/3}$ and satisfy (2.15) at each power of $\alpha^{1/3}$, which gives the unique solution

$$\eta(\phi) = e^{i\phi} - \sqrt[3]{\frac{16(\hat{\beta}^2 + 90)}{5\hat{\beta}^4 + 774\hat{\beta}^2 + 10935}}\, e^{-i\phi}\alpha^{2/3} + \mathcal{O}(\alpha^{4/3}), \tag{4.7}$$
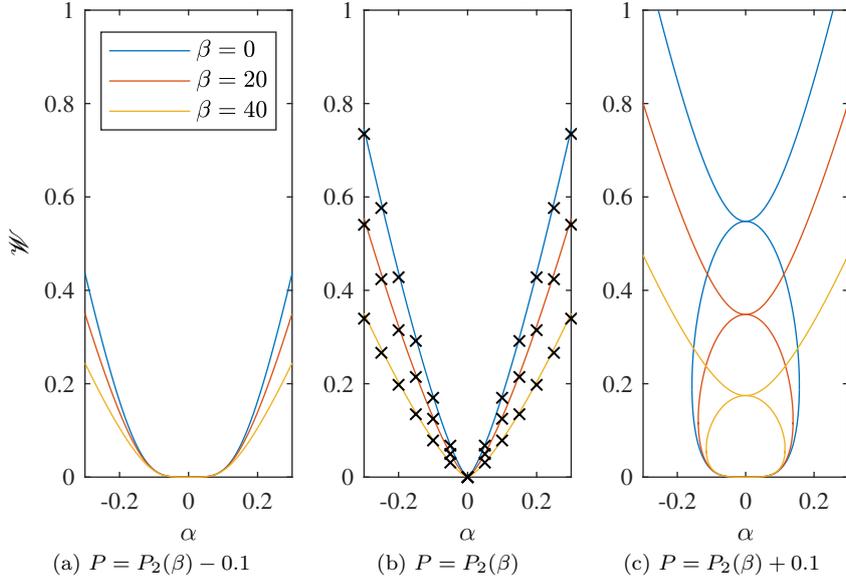
6

Figure 3: Numerically computed bending energy against α for solution branches near $P_2(\beta)$. The black crosses in (b) correspond to the analytical result (4.7) which is correct to $\mathcal{O}(\alpha^6)$.

where $\hat{\beta} = \beta/(2\pi)$, corresponding to an ellipse elongated vertically perpendicular to the flow. Note that at higher orders of α the circulation will induce a top-bottom asymmetry. Taking $\beta = 0$ we obtain $a_{1,1} = -\frac{2}{9}\sqrt[3]{12}$, which agrees with the results obtained by *et al.* [2]. As β is increased, the magnitude of the coefficient of $e^{-\mathrm{i}\phi}$ in (4.7) decreases and the cell becomes more circular.

Figure 3 shows the numerically computed bending energy against α for P near $P_2(\beta)$, along with the analytical results for $P = P_2(\beta)$. For $P < P_2(\beta)$ we find a single solution branch, with horizontally elongated cell shapes which are left-right symmetric. As the circulation is increased the bending energy of these cells decreases. These solution branches have $\mathscr{W} = 0$ at $\alpha = 0$, which corresponds to the circular solution. As P is increased to $P_2(\beta)$ the energy curve develops a cusp, as predicted by the expansion (4.7). We find excellent agreement between the analytical results and the numerical results for all values of β. As P is increased above $P_2(\beta)$ a loop appears in the energy curve underneath the previous solution branch, corresponding to cells which are vertically elongated. The solution branch containing the horizontally elongated cells no longer bifurcates from the unit circle at $\alpha = 0$, instead corresponding to the buckled mode-2 cell in a static fluid at $\alpha = 0$ with $\mathscr{W} > 0$. This change in orientation of the cells bifurcating from the unit circle at $\alpha = 0$ agrees with that predicted by (4.6).

We next consider the case where $P = P_3(\beta) = 8 + \hat{\beta}^2/4$. Using an integer power expansion of the form (4.2), we satisfy (2.15) at $\mathcal{O}(\alpha)$ to obtain $\sigma_1 = 0$ and $a_{n,1} = 0$ for $n \neq 2$, with $a_{2,1}$ undetermined. At $\mathcal{O}(\alpha^2)$, we find that $a_{2,1}$ satisfies

$$\left[(\hat{\beta}^2 + 140)(7\hat{\beta}^4 + 2580\hat{\beta}^2 + 64512)|a_{2,1}|^2 - 2\hat{\beta}^2(\hat{\beta}^2 + 252) \right] a_{2,1} = 0.$$

We thus have two distinct cases; either $a_{2,1} = 0$, or

$$|a_{2,1}| = \sqrt{\frac{2\hat{\beta}^2(\hat{\beta}^2 + 252)}{(\hat{\beta}^2 + 140)(7\hat{\beta}^4 + 2580\hat{\beta}^2 + 64512)}},$$
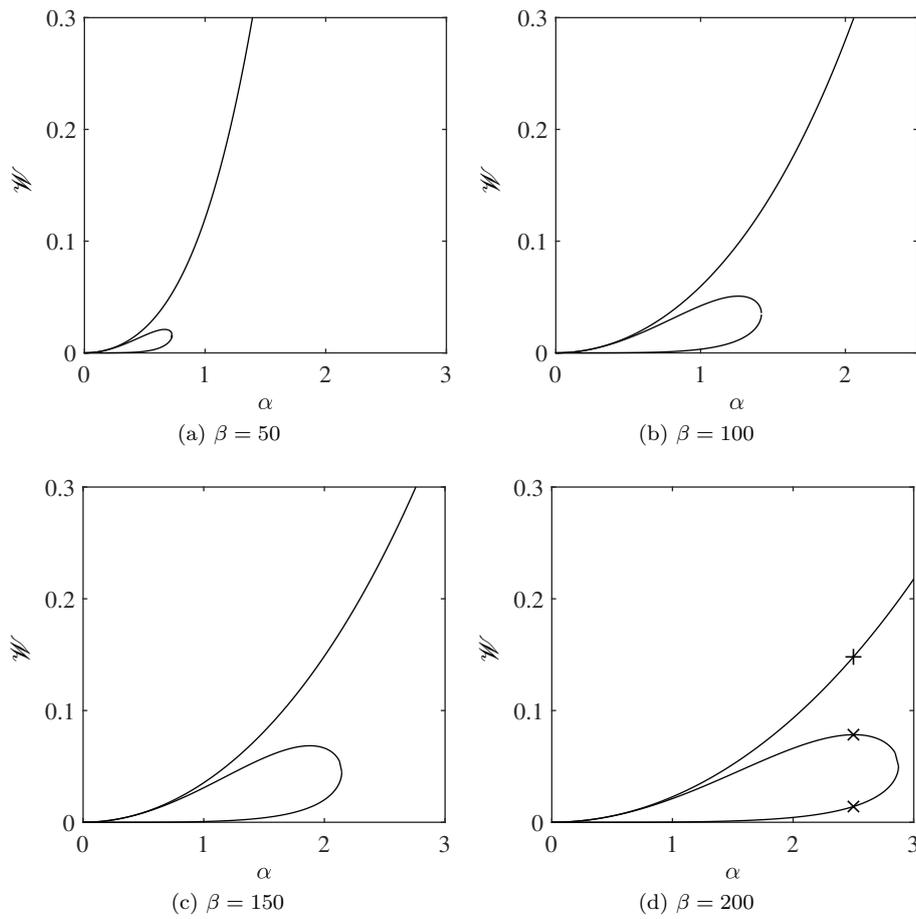
7

Figure 4: Bending energies of the solution branches at $P = P_3(\beta)$ against α for large β. The crosses in (d) correspond to the cell shapes depicted in Figure 5.
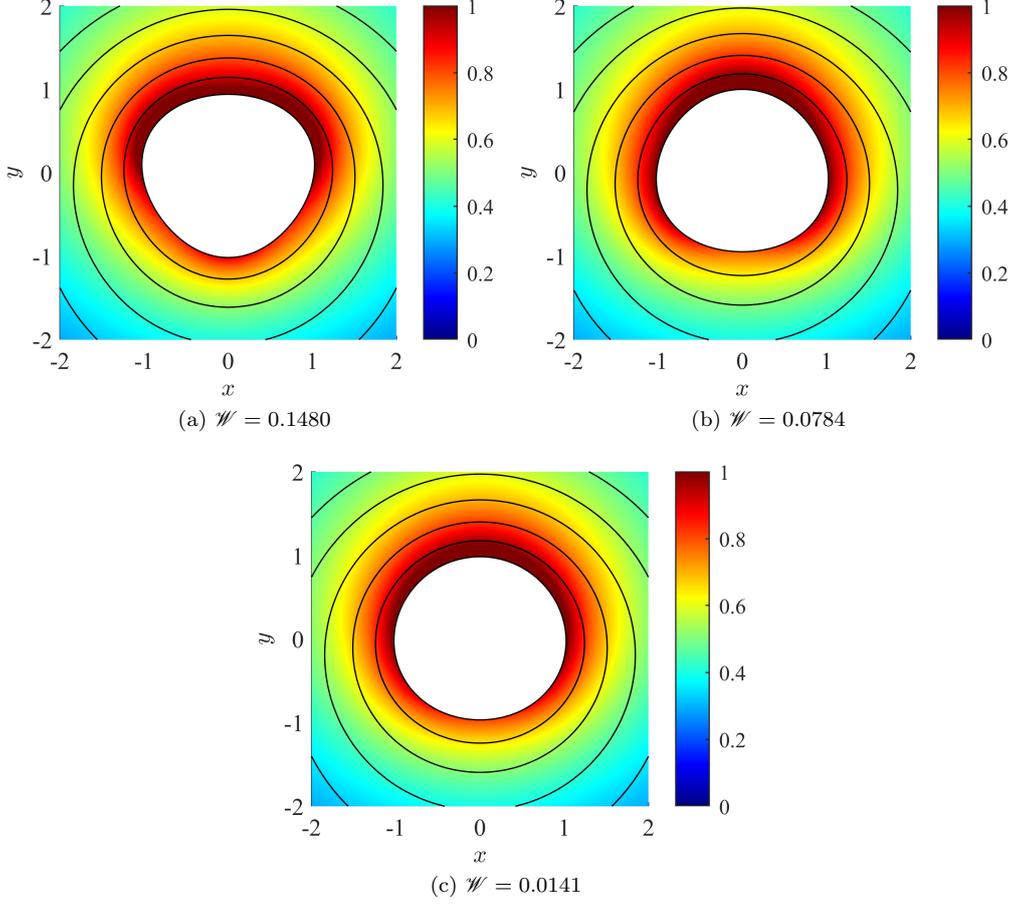
(a) $\mathscr{W} = 0.1480$

(b) $\mathscr{W} = 0.0784$

(c) $\mathscr{W} = 0.0141$

Figure 5: Contour plots of the flow past the three cells which exist for $\alpha = 2.5$, $\beta = 200$, $P = P_3(\beta)$, as shown in Figure 4d. The colour scale corresponds to the flow speed divided $\hat{\beta}$. The black lines are the streamlines of the flow.

with the argument of the complex coefficient $a_{2,1}$ undetermined at this stage. Each of these cases will correspond to a distinct branch of solutions.

Considering firstly the case where $a_{2,1} = 0$, we proceed to satisfy (2.15) at each power of α up to $\mathcal{O}(\alpha^5)$, at which point we obtain

$$\eta(\phi) = e^{i\phi} + \frac{4}{\hat{\beta}^2 + 60}\alpha^2 e^{-i\phi} - \frac{12(\hat{\beta}^2 + 105)}{\hat{\beta}(\hat{\beta}^2 + 60)^2}i\alpha^3 e^{-2i\phi} + \mathcal{O}(\alpha^4). \qquad (4.8)$$

At $\mathcal{O}(\alpha^2)$ the cell shape is elliptical with its major axis oriented horizontally in line with the uniform stream, with larger values of β corresponding to a more elongated shape. However, at $\mathcal{O}(\alpha^3)$ the cell becomes top-bottom asymmetric, although it retains a left-right symmetry. The $\mathcal{O}(\alpha^3)$ term has a singularity at $\beta = 0$; this solution is thus distinct from any which exists in the absence of circulation.

We then consider the case where

$$|a_{2,1}| = \sqrt{\frac{2\hat{\beta}^2(\hat{\beta}^2 + 252)}{7\hat{\beta}^6 + 3560\hat{\beta}^4 + 425712\hat{\beta}^2 + 9031680}}.$$
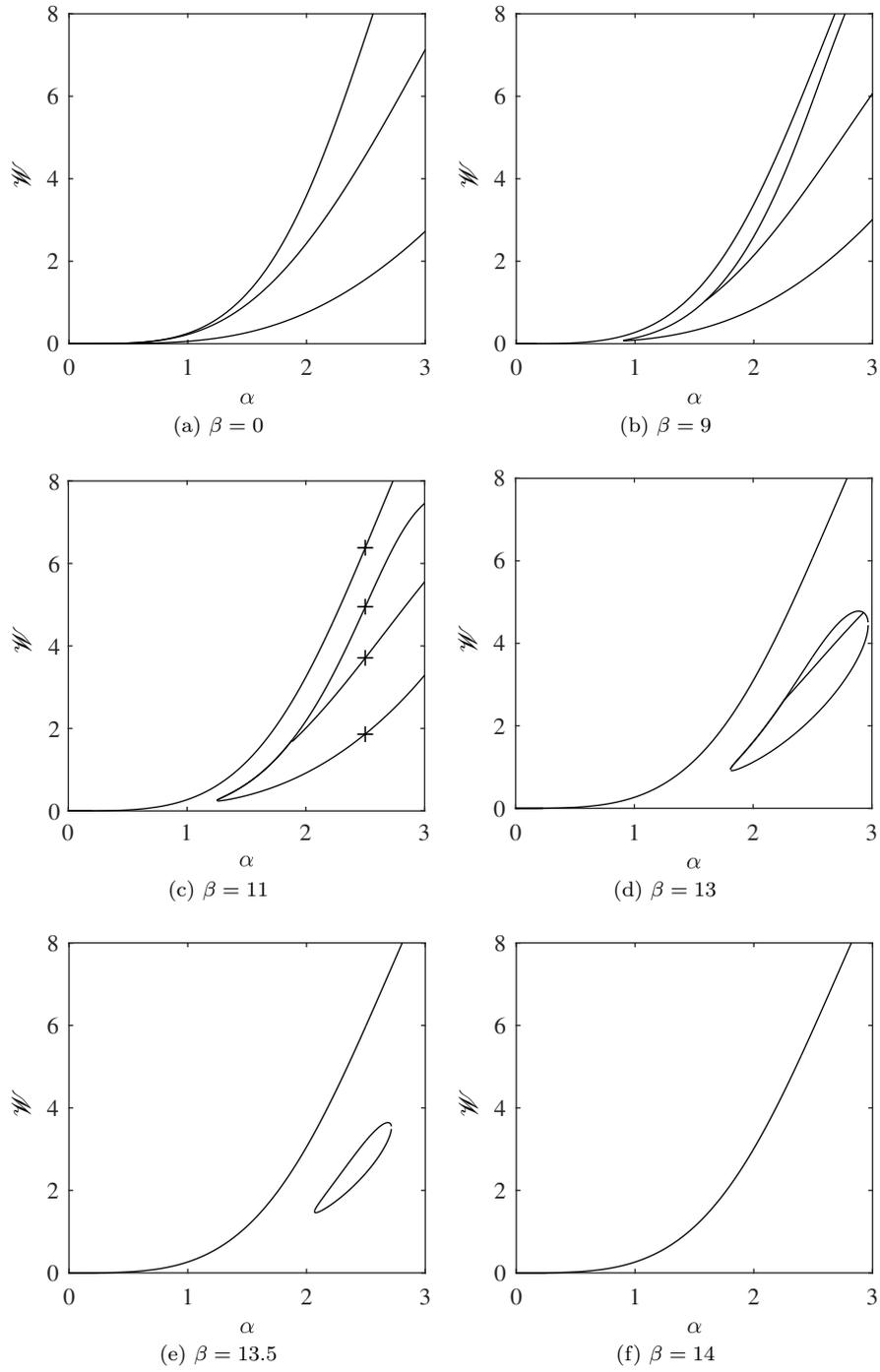
9

Figure 6: Bending energies of the solution branches at $P = P_3(\beta)$ against α for small β. The crosses in (c) correspond to the cell shapes depicted in Figure 7.

Satisfying (2.15) at $\mathcal{O}(\alpha^3)$, we find that $\Re(a_{2,1}\overline{a_{2,2}}) = 0$ while both $a_{2,1}$ and $a_{2,2}$ remain undetermined. At $\mathcal{O}(\alpha^4)$ we obtain $\Re(a_{2,1}) = 0$ and $\Im(a_{2,2}) = 0$, with $\Re(a_{2,2})$ undetermined. We thus have

$$a_{2,1} = \pm \mathrm{i}\sqrt{\frac{2\hat{\beta}^2(\hat{\beta}^2 + 252)}{7\hat{\beta}^6 + 3560\hat{\beta}^4 + 425712\hat{\beta}^2 + 9031680}},$$

which gives two distinct solutions depending on the sign of $a_{2,1}$. Finally, at $\mathcal{O}(\alpha^6)$ we find that $a_{2,2} = 0$, and obtain the value of $a_{2,3}$, which we omit for brevity. The solution is then given to $\mathcal{O}(\alpha^2)$ as

$$\begin{aligned}
\eta(\phi) &= \left(1 - |a_{2,1}|^2\alpha^2\right)e^{\mathrm{i}\phi} + \frac{4\alpha^2}{\hat{\beta}^2 + 60}e^{-\mathrm{i}\phi} \pm |a_{2,1}\alpha|\mathrm{i}e^{-2\mathrm{i}\phi} \\
&\pm \frac{4|ai2|\hat{\beta}\alpha^2}{3\beta^2 \hat{+} 420}e^{-3\mathrm{i}\phi} + \frac{\hat{\beta}^2 + 588}{3\hat{\beta}^2 + 756}|a_{2,1}|^2\alpha^2 e^{-5\mathrm{i}\phi} + \mathcal{O}(\alpha^3).
\end{aligned} \tag{4.9}$$

This cell is left-right symmetric but top-bottom asymmetric. At $\mathcal{O}(\alpha)$, the choice of sign of $\Im(a_{2,1})$ simply corresponds to a reflection of the cell shape about the x-axis. At higher orders of α however, the cell shapes differ at $\mathcal{O}(\alpha^2)$ depending on the sign of $\Im(a_{2,1})$.

The numerically obtained bending energies of the three solution curves bifurcating from the circular solution at $\alpha = 0$ for $P = P_3(\beta)$ for varying values of β are shown in Figure 4. We find that while solutions exist on the uppermost branch for all values of α, the lower two solution branches exist only for α below some maximum value. This maximum value of α increases as the circulation β is increased; however, the circulation β is always much greater than the maximum uniform flow speed α. Figure 5 shows the corresponding cell shapes and flow fields for $\alpha = 2.5$ and $\beta = 200$. The high circulation results in a near-circular cell, with the flow field resembling a vortex flow.

Figure 6 shows the bending energy of the solution branches for $P = P_3(\beta)$ for low values of β. For $\beta = 0$ we have the three solution branches described [2]. To describe the behaviour of the solution branches, we use the classifications defined in [2]. Cells on the lower branch, which are left-right and top-bottom symmetric, are classified as type 2a. Cells on the middle branch, which are top-bottom symmetric but left-right asymmetric, are classified as type 3a. Cells on the upper branch, which are left-right symmetric but top-bottom asymmetric, are classified as type 3b. Note that while the type 2a cells are left-right and top-bottom symmetric, the type 3a cells are left-right asymmetric and the type 3b cells are top-bottom asymmetric. Since the system for $\beta = 0$ is both left-right and top-bottom symmetric, the type 3a cells can be reflected horizontally to obtain another type 3a solution, and the type 3b cells can be reflected vertically to obtain another type 3b solution. As the circulation is then introduced the system loses its top-bottom symmetry; the type 3b solution branch thus splits into two separate branches, depending on the orientation of the cell. We classify the lower energy cell as type $3b_1$ and the higher energy cell as type $3b_2$. Plots of the cell shapes for each of these solution branches are shown in Figure 7.

For $\beta > 0$ the type 2a, 3a and $3b_1$ branches disconnect from $\alpha = 0$, remaining valid only for α above some minimum value. The type 2a and $3b_1$ branches, which both correspond to left-right symmetric cells, form a continuous loop in the $\alpha - \mathscr{W}$ plane, while the left-right asymmetric type 3a cells bifurcate from the type 2a–$3b_1$ loop. The solution branches shown in Figure 4 are also present for $\beta > 0$, but for low values of β these branches are too small to be seen.

As the circulation β is increased further we find that the type 2a–$3b_1$ branch forms a closed loop, with the solutions existing only for α between two critical values. The type
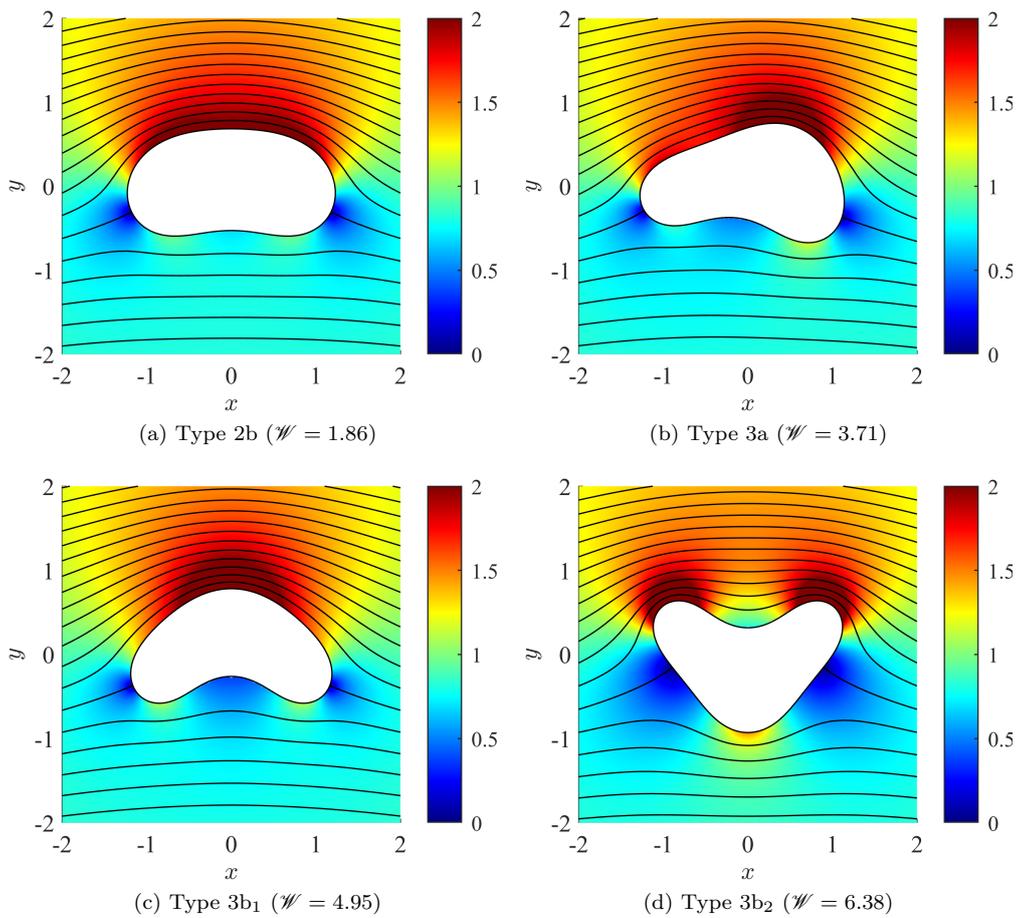
Figure 7: Contour plots of the flow past the three cells which exist for $\alpha = 2.5$, $\beta = 11$, $P = P_3(\beta)$, as shown in Figure 6c. The colour scale corresponds to the flow speed divided by the far-field flow speed α. The black lines are the streamlines of the flow.

3a solution branch is bounded by this closed loop, bifurcating from the 2a–3b$_1$ branch at both ends. This loop becomes smaller as β is increased, until approximately $\beta = 14$ where the loop disappears entirely, leaving only the type 3b$_2$ branch and those shown in Figure 4.

5. Summary

We have studied the deformation of an elastic cell in a uniform stream with circulation. Using a conformal mapping approach we have constructed asymptotic approximations for equilibria at low far-field flow speeds. We have computed nonlinear equilibria numerically and confirmed excellent agreement with the asymptotic approximations, and presented a detailed analysis of the nonlinear solutions.

Blyth & Părău [1] used a conformal mapping approach to study the deformation of an elastic cell in both a uniform stream flow and a vortex flow, and identified a set of critical transmural pressures at which buckled cells emerge. Yorkston *et al.* [2] subsequently used an asymptotic expansion based on a conformal mapping to study the cell deformation in a uniform stream, and presented an analysis of the full set of solution branches which emerge. We have expanded upon these studies by introducing a circulation to the flow, and presented an analysis of the complex solution space which emerges.

We have used asymptotic expansions for low flow speeds to obtain solutions which bifurcate from the unit circle. We obtained a general solution valid for general values of the pressure P and identified critical pressures at which distinct solution branches emerge. The general solution was found to be elliptical to first order, with the orientation depending on the pressure P; for P below the first critical pressure the cell is oriented vertically with its major axis perpendicular to the flow, while for P above the first critical value the cell is oriented horizontally with its major axis parallel to the flow. We found that as the circulation is increased the vertically oriented cells become more circular, while the horizontally oriented cells become more deformed. We found that the solution space near the second critical pressure becomes significantly more complex when the circulation is introduced. The solution branches which exist in the absence of circulation form a closed loop in solution space, which shrinks as the circulation is increased, while a set of novel solutions emerge for large circulation.

Yorkston *et al.* [2] performed a linear stability analysis along with nonlinear simulations of the unsteady flow to assess the stability of the equilibria for a flow with zero circulation. It would be informative to use a similar approach to analyse the stability of the new equilibria obtained here in the presence of circulation; this is left for future work.

References

[1] M. G. Blyth, E. I. Părău, Deformation of an elastic cell in a uniform stream and in a circulatory flow, IMA J. Appl. Math. 78 (2013) 665–684.

[2] A. A. Yorkston, M. G. Blyth, E. I. Părău, The deformation and stability of an elastic cell in a uniform flow, SIAM J. Appl. Math. 80 (1) (2020) 71–94.

[3] C. Pozrikidis, Numerical simulation of the flow-induced deformation of red blood cells, Ann. Biomed. Eng. 31 (2003) 1194–1205.

[4] D. A. Fedosov, M. Peltomäki, G. Gompper, Deformation and dynamics of red blood cells in flow through cylindrical microchannels, Soft Matter 10 (2014) 4258–4267.

[5] K. S. Chang, W. L. Olbricht, Experimental studies of the deformation of a synthetic capsule in extensional flow, J. Fluid Mech. 250 (1993) 587–608.

[6] Goodyear Aircraft, Summary: Report of the development of a one place Inflato-plane, Tech. Rep. GER 8146, Goodyear Aircraft (1957).

[7] D. Reasor, R. LeBeau, S. Smith, J. Jacob, Flight testing and simulation of a Mars aircraft design using inflatable wings, in: 45th AIAA Aerospace Sciences Meeting and Exhibit, 2012.

[8] A. D. Simpson, Design and evaluation of inflatable wings for UAVs, Ph.D. thesis, University of Kentucky (2008).

[9] M. Lévy, Mémoire sur un nouveau cas intégrable du problème de l'élastique et l'une des ses applications, J. Math. Pure Appl. 10 (1884) 5–42.

[10] G. F. Carrier, On the buckling of elastic rings, J. Math. Phys. 26 (1947) 94–103.

[11] I. Tadjbakhsh, F. Odeh, Equilibrium states of elastic rings, J. Math. Anal. Appl . 18 (1967) 59–74.

[12] J. E. Flaherty, J. B. Keller, S. I. Rubinow, Post buckling behavior of elastic tubes and rings with opposite sides in contact, SIAM J. Appl. Math. 23 (1972) 446–455.

[13] G. H. Halphen, Traité des fonctions elliptiques et de leurs applications, Gauthier-Villars, 1888.

[14] J.-M. Vanden-Broeck, J. B. Keller, Deformation of a bubble or drop in a uniform flow, J. Fluid Mech. 101 (1980) 673–686.

[15] P. N. Shankar, On the shape of a two-dimensional bubble in uniform motion, J. Fluid Mech. 244 (1992) 187–200.

[16] Q. Nie, S. Tanveer, The stability of a two-dimensional rising bubble, Phys. Fluids 7 (1995) 1292–1306.

[17] D. G. Crowdy, Circulation-induced shape deformations of drops and bubbles: exact two-dimensional models, Phys. Fluids 11 (10) (1999) 2836–2845.

[18] R. Wegmann, D. G. Crowdy, Shapes of two-dimensional bubbles deformed by circulation, Nonlinearity 13 (6) (2000) 2131–2141.

[19] C. Pozrikidis, Buckling and collapse of open and closed cylindrical shells, J. Eng. Math. 42 (2002) 157–180.

[20] S. Tanveer, Some analytical properties of solutions to a two-dimensional steadily translating inviscid bubble, Proc. R. Soc. Lond. A 452 (1996) 1397–1410.